Geologie en Mijnbouw 67: 333–348 (1988)

Textural evidence for seafloor, soft rock hydrothermal metamorphism in a garnet-scapolite-bearing metatuffite-exhalite-skarn-sphalerite ore sequence, Nora, Bergslagen, Sweden

I.S. Oen & R.H. Hellingwerf
Geological Institute, University of Amsterdam, Nieuwe Prinsengracht 130, 1018 VZ Amsterdam, The Netherlands

Received 3 August 1987; accepted in revised form 17 January 1988

Key words: seafloor metamorphism, diagenetic textures, exhalite-skarn-ore sequences, Bergslagen, Sweden

Abstract

Metatuffites in a skarn- and sphalerite ore-bearing metatuffite-exhalite sequence near Nora, Bergslagen, Sweden, have preserved the petrographic structure of a felsic tuff with quartz pyroclasts in a very fine-grained, strongly fractured and veined quartzo-feldspathic or sericite-rich matrix. Coeval differential compaction, recrystallization, and veining of tuffitic sediments is reflected by: parquet, rosette and parallel structures of micas; compaction-related 'ghost' veinlets, blind veinlets, and straight, folded, and refracted cross-veinlets; bending of schistosity around blind veinlets and quartz pyroclasts; rotation of pyroclasts in soft matrix; and compaction-controlled fracturing, veining, recrystallization and replacement of quartz pyroclasts, locally resulting in albite-quartz or carbonate-quartz pseudomorphs after the pyroclasts. Albite, garnet, scapolite, and other late mineral growths sequential to, but overlapping with the formation of the compaction-related structures, are indicated by: poikiloblasts in the pseudomorphs after quartz pyroclasts; late mineral growths in and along compaction-related veinlets; disseminated poikiloblasts traversed by compaction-related, often blind veinlets; and coarser grained bands and streaks of late minerals parallel to compaction banding. Garnet, scapolite, albite, carbonate, and other minerals show a layer-bound distribution. The paragenetic sequence of textures and minerals can be interpreted as the result of seafloor, soft rock hydrothermal metamorphism, involving interaction of different lithologies with hydrothermal fluids of rapidly changing PTX-characteristics, evolving from fluids in equilibrium with the host rocks to metasomatising fluids; these changes may be related to PTX-gradients around exhalative centres and interlayer rock-fluid-seawater-exhaled brine water interactions in unconsolidated tuffite-exhalite sediments.

Introduction

The Bergslagen region in central Sweden comprises a Mid-Proterozoic, 1.9–1.84 Ga plutono-volcano-sedimentary complex. The volcano-sedimentary rock unit in this complex is divided into a lower leptite group of mainly felsic volcanics, a middle leptite group of felsic volcanics, limestones, iron formations, cherts and other exhalative sediments and ores, and an upper leptite and slate group of felsic and basic volcanics, volcaniclastic shales and other tuffitic sediments, and local exhalative sediments and ores. The middle leptite and upper leptite and slate groups were deposited in long, nar-

row, mostly NW or N–S trending rift basins, e.g., the Saxån, Grythyttan, Ställdalen, and Nora basins (Oen, 1987).

The Nora basin stretches from about 20 km SW of the town of Nora in South Bergslagen for about 50 km to the NW. Between lakes Vikern and Älvlången, SW of Nora, the Nora basin is characterized by a steeply SE-dipping homoclinal succession of the middle leptite and upper leptite and slate groups (Hellingwerf *et al.*, 1988; see also Fig. 40). The lower part of the succession is dominated by felsic metavolcanic rocks; the higher part by thick marbles and metatuffites, with intercalated in the marbles a thin-bedded sequence consisting of marbles, siliceous, calcareous and pelitic metatuffites, vulcaniclastic shales and siltstones, and exhalite association lithologies (Plimer, 1986; Stanton, 1987) such as layers of various stratiform skarn rocks, sphalerite-galena ore-bearing strata, spessartine-rich siliceous rocks, cherts, tourmaline-biotite-garnet rocks, biotite rocks, garnetites, albitites, scapolite-rich rocks, iron formations, as well as barian and manganiferous horizons (Fig. 40).

This paper reports the conclusions of a thin section study of locally garnet- and scapolite-bearing, quartz pyroclast-rich felsic metatuffites in the Vikern-Älvlången tuffite-exhalite sequence.

General petrographic aspect of the metatuffites

Despite recrystallization, the metatuffites have generally preserved the structure of a felsic tuff, showing euhedral and angular quartz pyroclasts (to about 1 mm) in an equigranular matrix of ash-size (usually between 0.01 and 0.1 mm) grains of quartz, albite, and K-feldspar, with minor biotite, muscovite, carbonate, amphibole, and accessory minerals.

The quartz pyroclasts are in part recrystallized and locally replaced by carbonate, albite, muscovite, garnet and scapolite. The matrix is massive, banded, or schistose. The alternation of coarser and finer grained layers of somewhat different compositions reflects differences in composition and grain size of the original tuff layers. The tuffitic sequences in the Bergslagen rift basins generally show well preserved sedimentary structures such as graded and cross bedding and load casts (Kuipers, 1987). Some structures, such as normal faults and diapiric folds resembling water escape structures, are reminiscent of soft rock deformation structures (Davison, 1987; Van Loon & Brodzikowski, 1987). Schistosity is due to the orientation of mica flakes, usually parallel, but sometimes also oblique to the layering. Some metatuffites have a matrix of massive or schistose sericite or muscovite. The metatuffites are traversed by abundant veinlets, parallel to and across the layering.

Parquet, rosette, and parallel structures of micas related to compaction

The metatuffites show alternations of very fine (0.01–0.03 mm) and fine-grained (up to about 0.1 mm), massive and schistose quartzo-feldspathic and sericite-muscovite layers. Massive quartzo-feldspathic layers show granular quartz and feldspars and flaky biotite and/or muscovite in random orientation; schistose quartzo-feldspathic layers show flat quartz and feldspar between parallel orientated micas (Figs 17, 19–22, 32). Massive and weakly schistose sericite-muscovite layers show a network of interlocking mica flakes in parquet structure (flakes in two directions at about 45° to the layering; Figs 23–26, 35–38) and rosette structure (flakes at about 45° and parallel to the layering; Figs. 9–10); schistose sericite-muscovite layers show a dense mass of parallel orientated micas (Figs. 1–5).

The preservation of quartz pyroclasts in massive as well as schistose layers, and other structures described below, suggest that the variation in mica fabrics from random orientation in massive layers, to parquet and rosette structures in weakly schistose layers, and parallel structure in strongly schistose layers, is related to differential compaction of soft tuffitic sediments (the more schistose layers showing the stronger compaction) rather than to tectonic compression. Parquet and rosette structure of stilpnomelane in Australian banded iron formations and in exhalite–type skarns of the Grythyttan basin have previously been interpreted

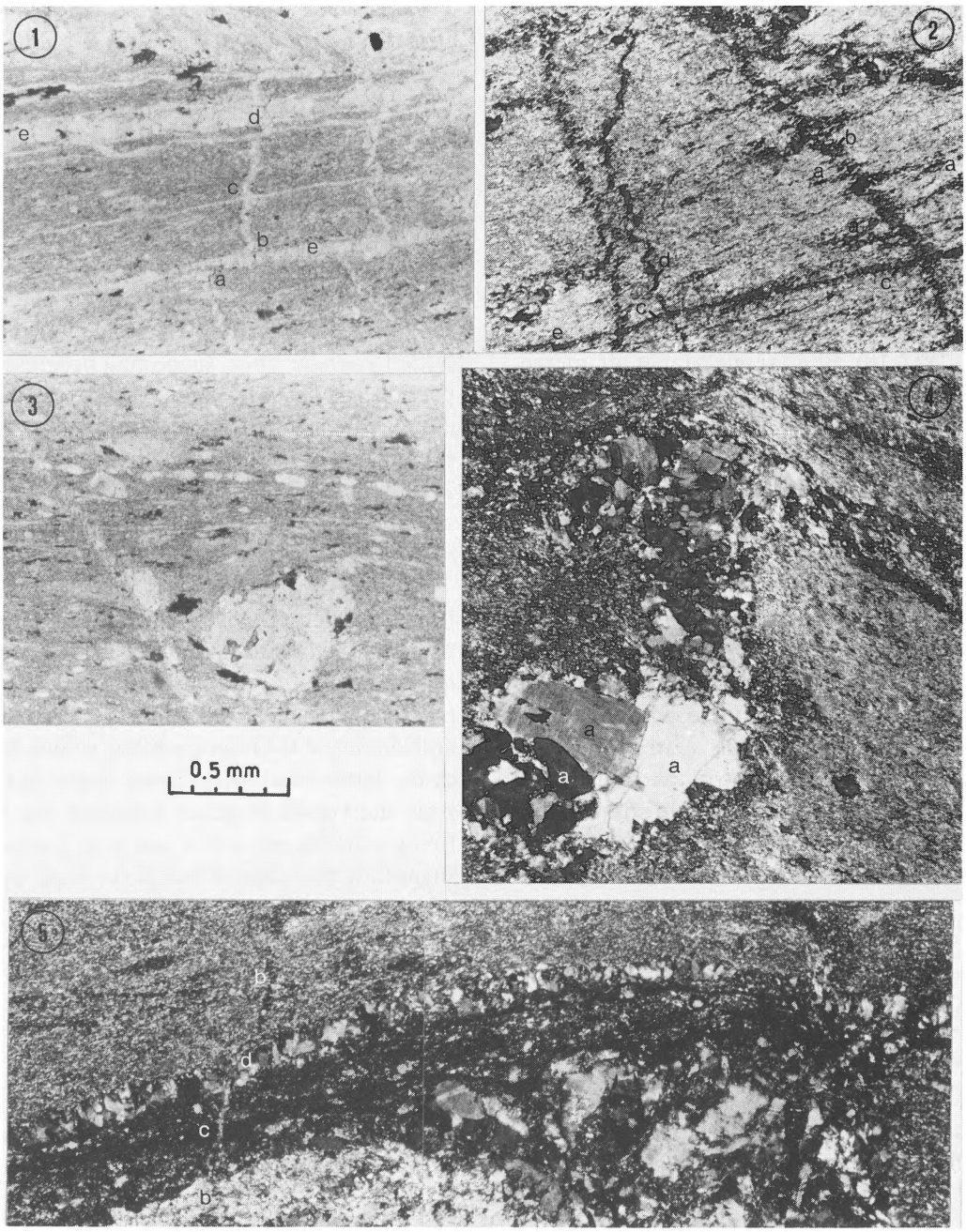

Figs. 1–5. Sericite-rich metatuffite, slide 56. 1. Schistose sericite band shows quartz-feldspar net-veining by compaction-folded cross-veinlets and schistosity-parallel veinlets; cross-veinlets taper off before intersection with, (*a*), abut against, (*b*), are intersected by, (*c*), and intersect, (*d*), parallel veinlets; parallel veinlets are broken by small blind cross-veinlets (*e*); parallel nicols. 2. Folded quartz-feldspar cross-veinlets indicating progressive compaction of sericite matrix and coeval veining; strongly folded cross-veinlet *a* is intersected by folded cross-veinlet *b*, which is intersected by parallel veinlet *c*; relatively weakly folded cross-veinlet *d* intersects veinlet *c*, which is also off-set by normal fault *e*; crossed nicols. 3. Schistosity-parallel quartz-feldspar swells and an albitized quartz pyroclast showing original form; compaction-related bending of schistosity around pyroclast; parallel nicols. 4 and 5. Compaction-related bending of sericite schistosity around tips of blind veinlets; albite porphyroblasts (*a*) in buckled blind quartz-feldspar veinlet; differential compaction shown by small cross-veinlet which is folded (*b*) in sericite bands and straight (*c*) in less compacted quartzo-feldspathic band; small veinlet is off-set by schistosity-parallel dilatation veinlet *d*; crossed nicols. All figures on same scale.

as diagenetic textures by Miyano (1982) and Oen *et al.* (1986), respectively.

Fracturing and veining related to compaction

Veinlets with quartz, feldspars, carbonate, micas, and other minerals occur across and parallel to the layering and fine banding in the metatuffites. Many cross-veinlets are short, blind veinlets across one or a few thin bands, and sometimes across single mineral grains (Fig. 18). Blind veinlets taper off, merge into, or abut against rock bands or banding-parallel veinlets (Figs. 1, 4, 5). Many veinlets are overgrown by the matrix or are filled with minerals that are the same and have similar grain size as those of the matrix. These veinlets appear as vague 'ghost' veinlets. Figure 17 shows regularly spaced, straight quartz-rich 'ghost' veinlets in a quartz-feldspar-biotite matrix; the veinlets are discernible only by discontinuous trains of similarly orientated quartz grains marking biotite-free fracture-fillings in the biotite-rich matrix. Quartzo-feldspathic 'ghost' veinlets in quartzo-feldspathic matrix, sericitic 'ghost' veinlets in sericitic matrix, and carbonate 'ghost' veinlets in carbonate rocks, are often vaguely visible under crossed nicols in certain positions of the stage. The more conspicuous veinlets show minerals, grain size and/or texture, contrasting with that of the matrix (e.g., granular quartz-feldspar veinlets in schistose sericite matrix, Figs. 1–5). The ubiquity, abundance, and often net-like pattern (Fig. 1) of veinlets and 'ghost' veinlets suggest intensive fracturing and soaking with fluids. Banding-parallel quartz-feldpar swells (Fig. 3) and dilatation veinlets (Fig. 5) suggest relatively high fluid and low lithostatic pressures, enabling dilatation normal to fluid-overpressured bedding planes; the dilatation veinlets show columnar growths of quartz and feldspars normal to the banding-parallel vein walls and dilation off-set of transected veinlets. The described conditions commonly prevail during dewatering and compaction of soft sediments. Contemporaneous compaction and veining is shown by folded veinlets, refracted veinlets, and other structures described below.

An effect of compaction is the folding of cross-veinlets with axial planes of the folds always straight and parallel to the schistosity, whatever the intensity of folding and orientation of the veinlet. This suggests only one direction of shortening, i.e. normal to bedding and schistosity as in compacting sediments (Davison, 1987).

The metatuffites show many compaction-related microstructures that resemble the compaction-related mesoscopic structures described by Davison (1987) in a sandstone-siltstone sequence. Figure 2 shows folded older veinlets beside less intensively folded younger ones, suggesting progressive compaction and coeval veining. Figure 5 shows differential compaction of sericitic and quartzo-feldspathic bands: a cross-veinlet is folded in the stronger compacted sericitic bands, but yet almost straight in a less compacted quartzo-feldpathic band.

Differential compaction is also shown by refraction of veinlets (Davison, 1987). Figure 39 shows a tremolite-actinolite veinlet crossing a banded quartz-feldspar-tremolite rock; a stronger compacted quartz-feldspar band has caused refraction and kinking of the fracture-filling veinlet as it crosses the latter band under lower angle; in the kink-zone the veinlet is rather indistinct, the fracture-filling minerals spread out and form coarser grains, suggesting that compaction of the band was coeval with fracture-filling.

Some folded cross-veinlets show displacement of the layering and banding, indicating that they were fracture-fillings of fault planes in compacting sediments (Fig. 2).

Bending of schistosity around blind veinlets and pyroclasts related to compaction

Davison (1987) has described compaction of a sandstone-siltstone sequence resulting in buckling and probably rotation and thickening of sandstone dykes in shale layers, and in bending of shale bedding planes around sandstone balls and pillows. The blind quartz-feldspar veinlets in Fig. 4 and 5 were buckled and thickened by compaction of the sericitic matrix, in a similar way as the sandstone dykes of Davison (1987). The bending of schistosity

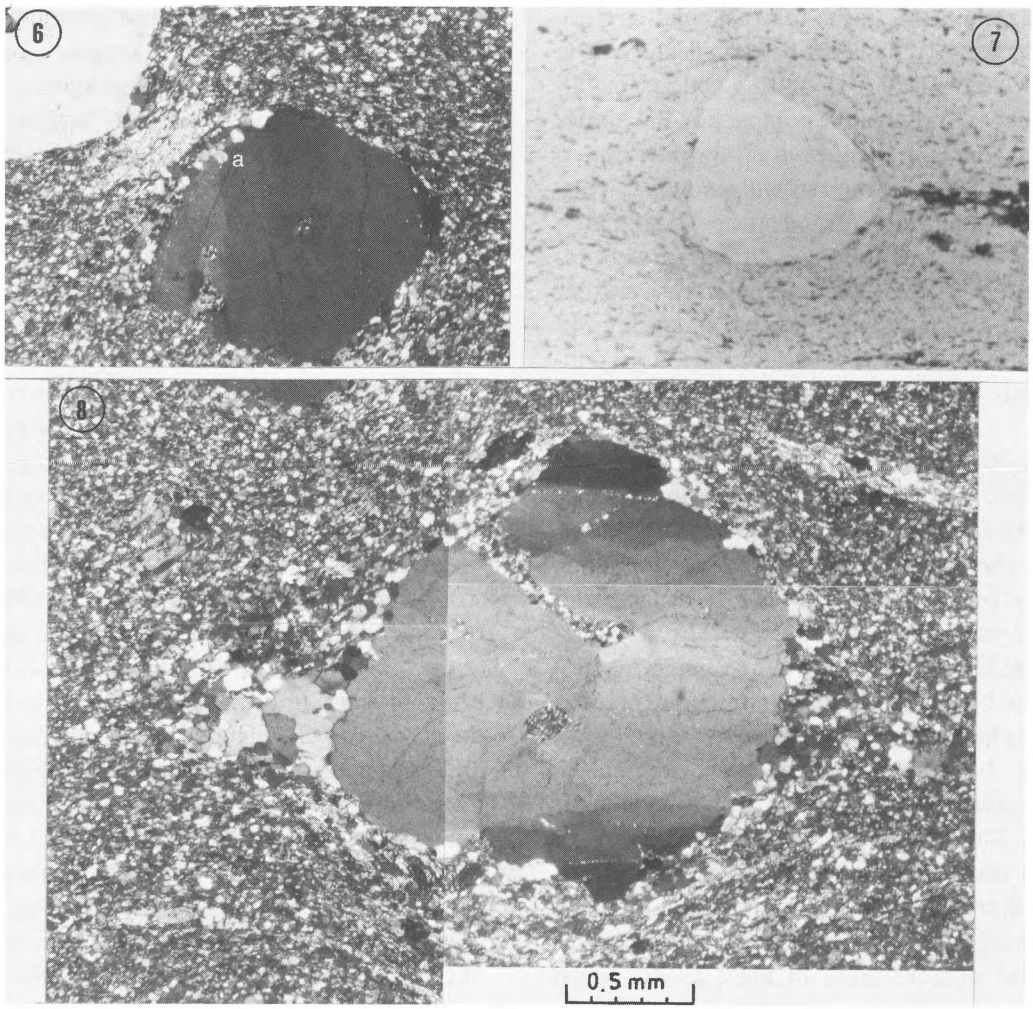

Figs. 6–8. Quartzo-feldspathic metatuffite, slide 102. 6. Compaction-related bending of schistosity around euhedral quartz pyroclast; fine cracks filled with mineral particles; lamellar subgrain formation; beginning grain boundary recrystallization at one side (*a*); crossed nicols. 7. Compaction-related bending of schistosity around quartz pyroclast; schistosity defined by biotite flakes (dark); parallel nicols. 8. Compaction-related bending of schistosity around rounded quartz pyroclast; lamellar subgrain formation especially at strained tips of pyroclast is superimposed on polygonal crack system with particle linings; some cracks are opened and filled; grain boundary recrystallization of quartz and outgrowth of quartz aggregates at pressure-shadow sides of pyroclast; crossed nicols. All figures on same scale.

around the tips of blind veinlets is ascribed to the stronger compaction of the matrix relative to the veinlets. A similar effect of differential compaction is shown by the bending of schistosity around quartz pyroclasts (Figs. 6–8, 19–20), resulting in microstructures resembling the mesoscopic ball-and-pillow structures of Davison (1987).

Quartz pyroclast fracturing and recrystallization related to compaction

The compaction structures around quartz pyroclasts indicate that vertical compressive stresses were initially taken up by compaction of the matrix. This matrix was a more or less clay-altered felsic tuff, which responded to burial and compaction by loss of water, hydraulic fracturing, and

recrystallization in quartz-feldspar and sericite rocks. The softer the matrix the longer the quartz pyroclasts can withstand fracturing and recrystallization, but with progressive compaction the matrix gains strength, and changes in strain distribution between matrix and pyroclasts will result in fracturing and recrystallization of the latter. The intimate association of unfractured and strongly fractured, and of unrecrystallized and completely recrystallized quartz pyroclasts suggests that fracturing and recrystallization of the pyroclasts occurred contemporaneously with consolidation of the compacting rocks.

Figures 35–38 show unfractured and fractured, euhedral and angular quartz pyroclasts in one slide. The quartz-albite-rich fracture fillings can be followed in the sericite matrix as 'ghost' veinlets, crossing several fractured quartz pyroclasts and abutting against unfractured ones (Fig. 38). Figures 34 and 33 show fracture-filling veinlets that are interrupted by unfractured and strained quartz pyroclasts, respectively. Feldspar pyroclasts are absent, but biotite-muscovite-chlorite aggregates may represent pseudomorphs after clay-altered feldspars. The quartz pyroclasts were apparently alteration-resistent, strong particles in a more or less clay-altered, soft matrix with rheological properties varying from ductile to brittle. Soft deformation is also demonstrated in Figs. 21–22, which show that hard pyroclasts in a soft matrix were rotated into a position with longest dimensional axis at an oblique angle to the schistosity.

Figures 9–13 show incipiently and completely recrystallized, smaller and larger quartz pyroclasts in one slide. Incipient modification of the pyroclasts is marked by a polygonal pattern of cracks, sealed by recrystallized quartz and linings of albite, muscovite and carbonate particles (Figs. 8, 9, 11). A lamellar pattern of incipient subgrains is superimposed on the polygonal crack system (Figs. 8–9). These cracks are early structures, which possibly may be related to the clay-alteration processes. Euhedral quartz pyroclasts often show subgrain development and grain boundary recrystallization beginning at tips of the crystals that protrude into the schistosity and that were subjected to stronger strain under the compactional stresses (Figs. 6–8). In some examples outgrowths of quartz aggregates at the pressure shadows of the pyroclasts suggest a pressure-solution process resulting in rounding of the clasts (Fig. 8). Figure 9 shows advanced quartz grain boundary recrystallization, and Figs. 10 and 12 complete quartz grain recrystallization. In many quartz pyroclasts some of the polygonal cracks are widened and injected with matrix material; the wider cracks are filled with relatively coarse-grained quartz and/or albite and/or muscovite and/or carbonate (Fig. 11). Often relatively broad vein-

→

Figs. 9–13. Muscovite-rich metatuffite, slide 100. 9 and 10. Parquet- to rosette-structured muscovite-rich matrix, muscovite flakes at about 45° and parallel to the bedding (parallel to short side of picture); fig. 9 shows polygonal cracks with particle linings in quartz pyroclasts and superimposed lamellar subgrain formation and grain boundary recrystallization; fig. 10 shows completely recrystallized quartz pyroclast (*a*). 11. Quartz pyroclast showing polygonal cracks with particle linings; incipient formation of veinlets by widening and filling of cracks with quartz and muscovite. 12 and 13. Recrystallized quartz pyroclasts; larger relict grains show polygonal cracks and undulatory extinction; fig. 13 shows pyroclast cut in two parts by blind veinlet of quartz and muscovite. All figures with crossed nicols and one same scale.

Figs. 14–16. Carbonate-bearing metatuffite, slide 103. 14. Recrystallized quartz pyroclast showing incipient fragmentation due to grain boundary replacement and veining by quartz-carbonate-muscovite. 15. Quartz pyroclast showing advanced stage of fragmentation by carbonate-quartz-muscovite veinlets; relict quartz fragments show polygonal fractures and undulatory extinction. 16. Quartz pyroclast largely replaced by carbonate; *q* relicts of quartz. All figures with crossed nicols and on same scale.

Figs. 17–18. Garnet-bearing metatuffite, slide 532. 17. Schistose biotite-rich quartzo-feldspathic matrix with vaguely visible thin quartz-feldspar 'ghost' veinlets in the direction *a–b*; garnet poikiloblast in carbonate-quartz pseudomorph (*c*) after quartz pyroclast; epidote veinlet e overprinting old 'ghost' veinlet; small garnet skeletons and epidote granules in the matrix; parallel nicols. 18. Blind carbonate veinlet in garnet poikiloblast in carbonate-quartz pseudomorph after quartz pyroclast; crossed nicols. All figures on same scale.

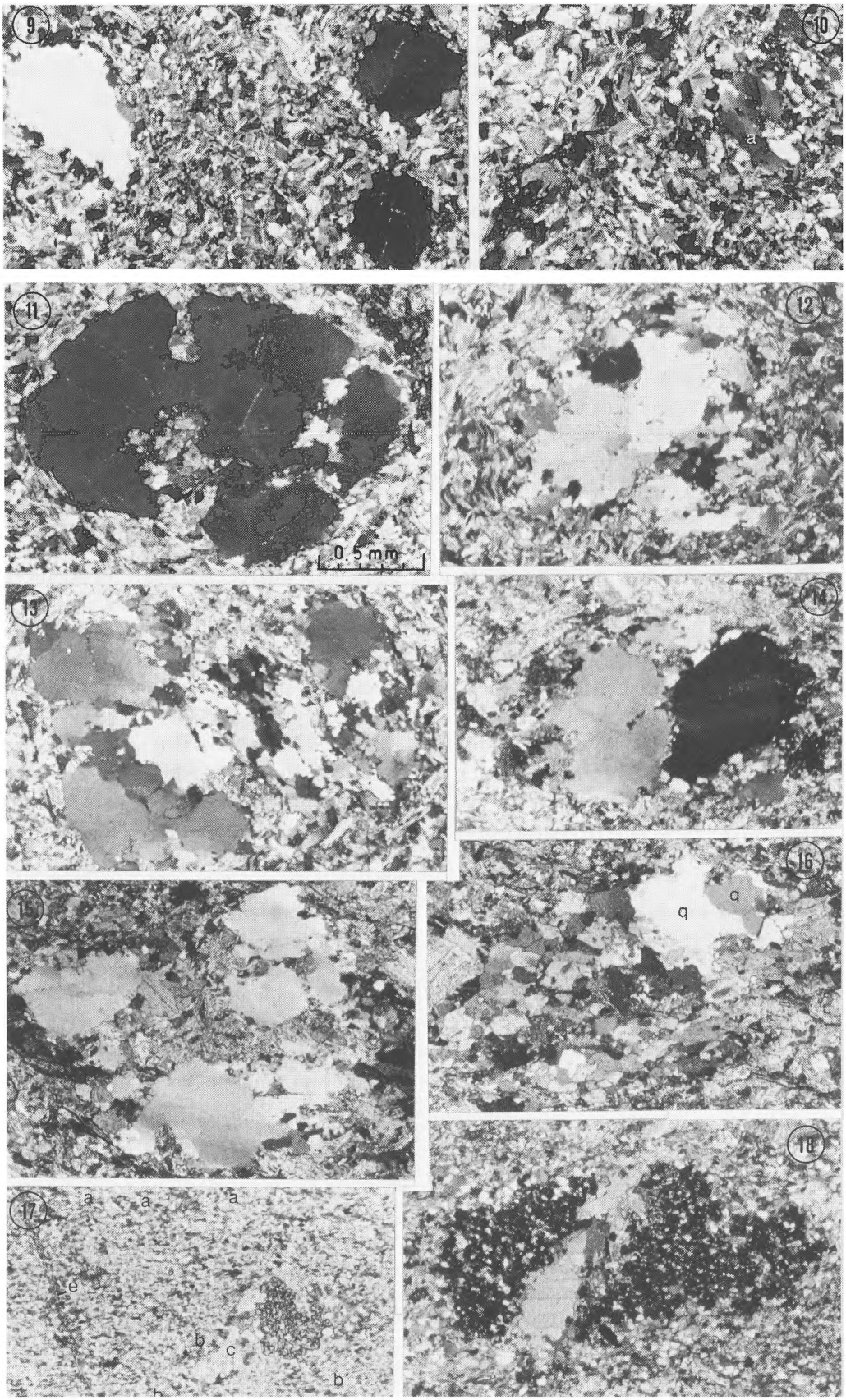
9
10
a
11
0.5 mm
12
13
14
15
16
q
q
17
a
a
a
e
b
c
b
b
18

lets and rims of the latter minerals are formed, and the quartz pyroclast is broken into fragments. However, the original outline of the pyroclast is often still preserved; in some cases the recrystallized pyroclasts form more or less rounded aggregates marked by the bending of schistosity and development of biotite around the aggregates, as also observed around unrecrystallized quartz pyroclasts. Figure 13 shows a recrystallized quartz pyroclast cut in two parts by a quartz-muscovite blind veinlet; Fig. 14 shows relicts of a fragmented quartz pyroclast enclosed in a quartz-carbonate aggregate and traversed by a thin quartz-carbonate blind veinlet; Fig. 15 shows quartz pyroclast fragments in a carbonate aggregate; and Fig. 16 shows almost complete replacement of a quartz pyroclast by carbonate.

In other examples, albite is the replacing mineral. Figures 19, 20, and 23 show grain boundary replacement of quartz pyroclasts by albite; partly albite-replaced quartz pyroclasts occur besides completely unaffected and completely replaced ones. The latter consists of granular albite or albite-quartz pseudomorphs after the pyroclasts (Figs. 19–24); some of the pseudomorphs contain granules of tourmaline, allanite and sphene. The latter minerals also occur in albite-rich veinlets in the rock. The replacement of quartz pyroclasts presumably involves a pressure-solution process in the presence of fluids of different PTX-characteristics; quartz is recrystallized when under the prevailing conditions it is less soluble than albite, carbonate, and muscovite, whereas it is replaced by the latter minerals when it is more soluble.

Albite, garnet, and scapolite blastesis related to quartz pyroclast recrystallization

Figures 25–28 show stages in the development of subhedral to euhedral albite poikiloblasts in granular albite pseudomorphs after quartz pyroclasts. The albite blasts enclose granular albite and develop smooth crystal faces against the granular matrix (Fig. 25), indicating that they are recrystallization products of the granular albite and not relics of recrystallized albite pyroclasts. Moreover, the albite blasts occur in rocks which show other signs of albitization such as coarser albite in the matrix, albite streaks, and albite blasts in quartz-feldspar veinlets (Fig. 4).

Garnet and scapolite show a similar textural development as the albite poikiloblasts. Some metatuffite layers show relatively large garnet poikiloblasts in quartz-carbonate pseudomorphs after quartz pyroclasts, and smaller skeletal grains of garnet in the matrix (Figs. 17–18). The garnet poikiloblast in Fig. 18 is traversed by a blind carbonate veinlet in a similar way as the recrystallized quartz pyroclasts in Figs. 13–15 are traversed by blind veinlets. This suggests that quartz pyroclast recrystallization and garnet poikiloblastesis may be related sequential processes. The garnets in the matrix are surrounded by epidote granules, while epidote also occurs in veinlets along and parallel to quartz-feldspar 'ghost' veinlets (Fig. 17) and across garnet poikiloblasts in the pseudomorphs after pyroclasts. The sequence of textures and minerals suggests that fracturing and recrystallization of matrix and pyroclasts were associated with changes in character of the rock fluids. The initial quartz-feldspar-sericite-precipitating fluids were presumably in equilibrium with the rock; the later fluids were metasomatising fluids, changing rapidly from carbonate- to garnet-, and to epidote-precipitating.

→

Figs. 19–22. Albite-rich metatuffite, slide 104. 19 and 20. Same view with parallel and crossed nicols; quartz pyroclast *a* shows grain boundary replacement by albite, pyroclast *b* is altered into a granular albite-quartz pseudomorph, *c* is a small albite blast in the matrix; compaction-related bending of schistosity around pyroclasts. 21 and 22. Same view with parallel and crossed nicols; granular albite and albite-quartz pseudomorphs after quartz pryoclasts; tourmaline, epidote, allanite, and sphene in pseudomorphs; rotation of pyroclasts is indicated by parallel arrangement of pseudomorphs with longest dimensional axis oblique to the schistosity; subhedral albite porphyroblast *a* in granular albite pseudomorph. All figures on same scale.

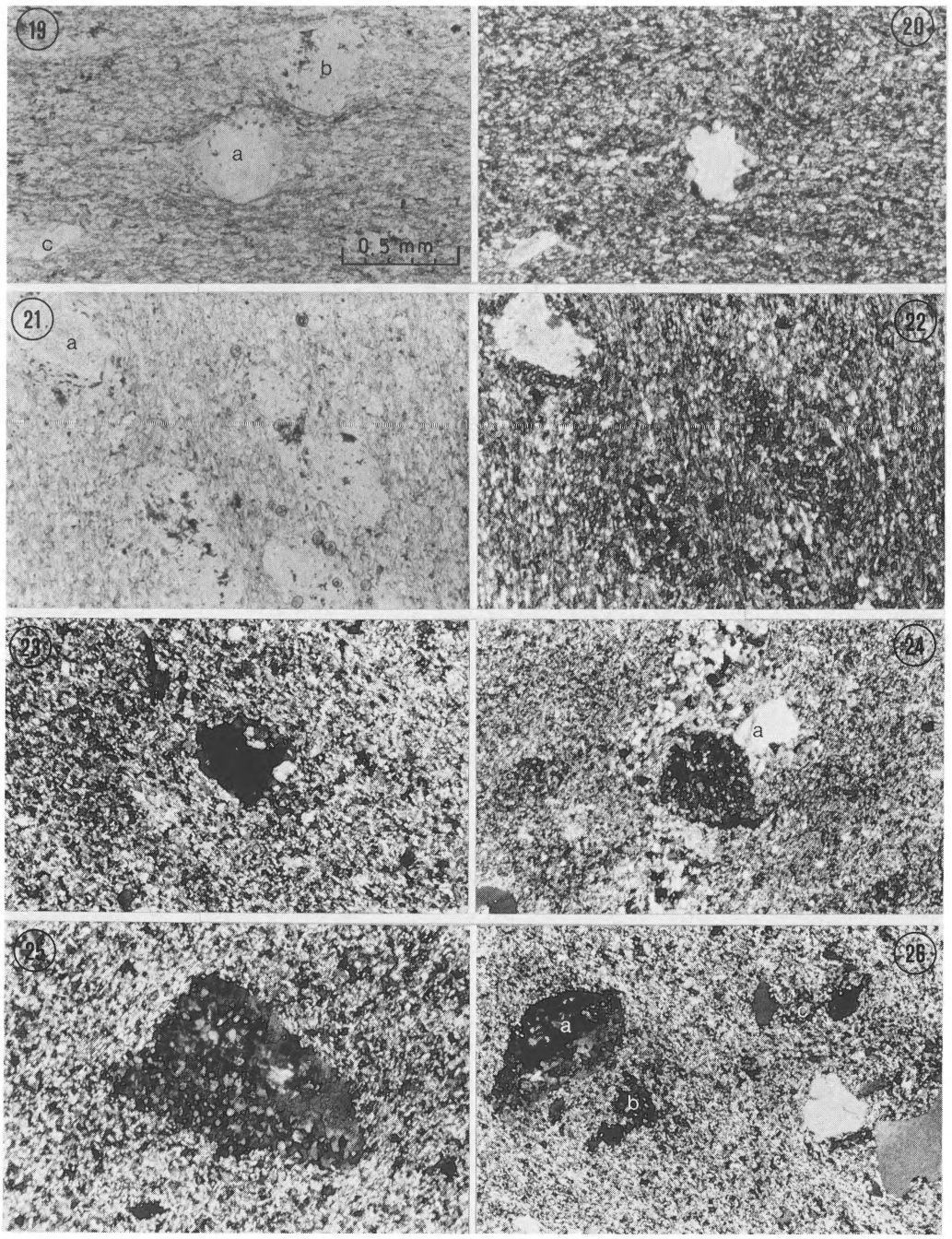

Figs. 23–26. Sericite-rich metatuffite, slide 572. 23. Quartz pyroclast showing grain boundary replacement by granular albite; parquet structure of sericite in matrix. 24. Granular albite-quartz pseudomorph is unaffected by a later quartz-albite veinlet; adjacent pyroclast *a* is fractured and veined. 25. Albite poikiloblast has developed crystal faces in a granular albite pseudomorph; parquet structure of sericite in matrix. 26. Subhedral albite poikiloblast *a* has replaced a granular albite pseudomorph; *c* is a biotite-chlorite-sericite aggregate, possibly a pseudomorph after a feldspar pyroclast; note fresh quartz pyroclasts and parquet structure of sericite. All figures with crossed nicols and on same scale.

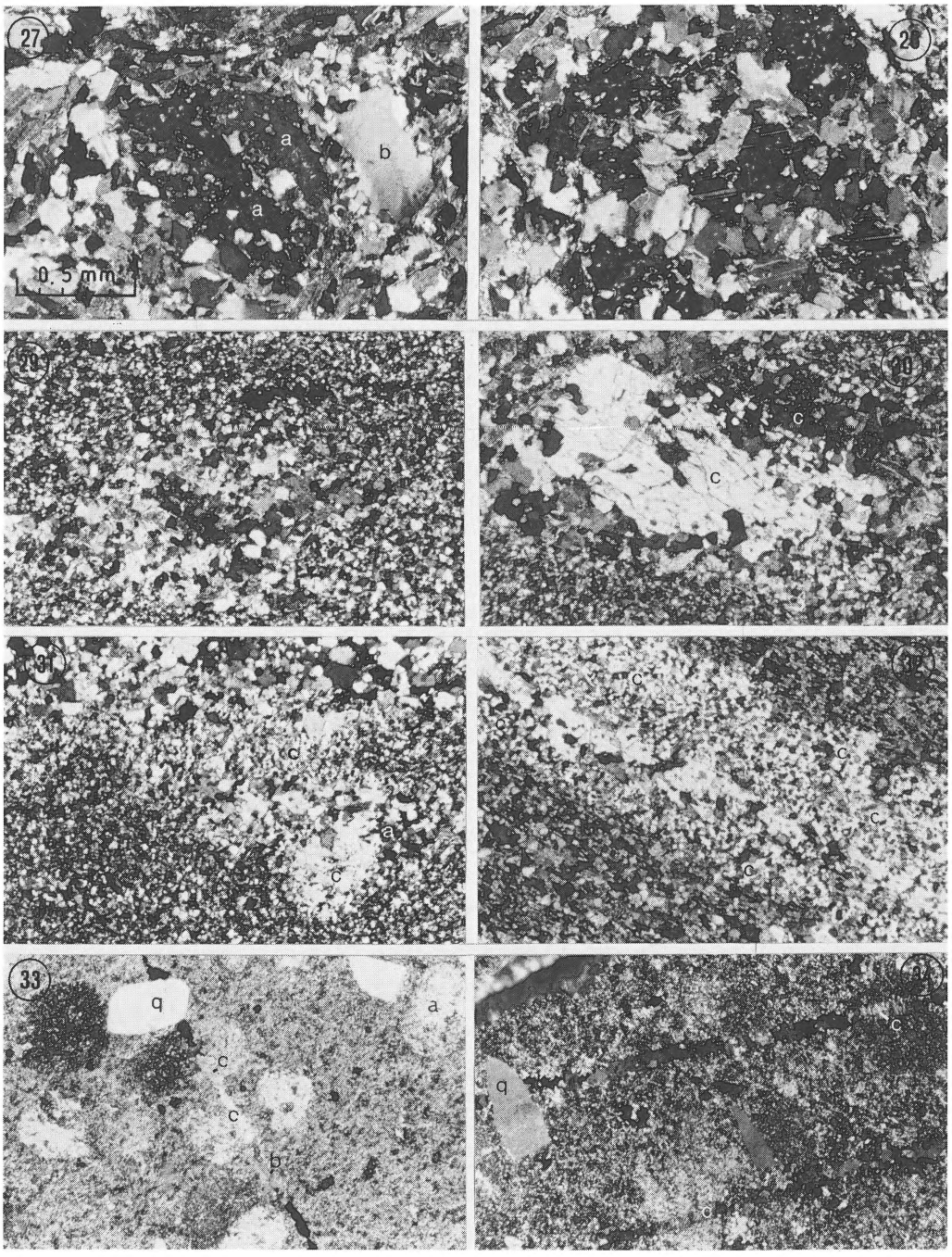

Figs. 27–28. Albite-rich metatuffite, slide 609. 27. Subhedral albite poikiloblast *a* in recrystallized quartz pyroclast; *b* relic of quartz pyroclast. 28. Subhedral albite poikiloblast in coarse granular quartz-albite pseudomorph after quartz pyroclast. All figures with crossed nicols and on same scale.

Figs. 29–32. Scapolite-bearing metatuffite, slide 513B. 29 Quartz-carbonate pseudomorph after quartz pyroclast in quartz-feldspar-biotite matrix. 30. Scapolite poikiloblasts (*c*) in quartz-carbonate pseudomorph. 31. Scapolite poikiloblasts (*c*) along boundary of finer and coarser grained metatuffite bands and in a quartz-carbonate pseudomorph (*a*). 32 Poikiloblastic scapolite (*c*) outgrowths along a banding-parallel scapolite-filled veinlet. All figures with crossed nicols and on same scale.

Garnet bands have not been observed in metatuffites, but they are frequent in skarn and biotite rocks in the same sequence, showing textures similar to those described by Stanton (1976, 1987) in the Broken Hill deposits and stratiform skarns in Australia. Microprobe analyses indicate essentially almandine-spessartine garnets with almandine contents varying strongly between layers from about 75 mol.% to about 45 mol.%.

Scapolite is observed in some metatuffite layers as peculiar poikiloblasts. In some of the scapolites spotty micaceous alteration around zircon- or allanite-like inclusions gives a false impression of pleochroic halos. Other scapolite crystals show six-sided sections, often with a sector structure as in sector-twinned cordierite (Fig. 35). In fact, these scapolites of peculiar habit were erroneously identified as cordierite until subsequent X-ray powder and microprobe determinations proved that the mineral was scapolite of marialite to dipyre composition (with up to about 40 mol.% meionite).

The scapolite occurs in some of the metatuffite layers as poikiloblasts in quartz-carbonate pseudomorphs after quartz pyroclasts (Figs. 29–31), in scapolite-quartz-feldspar-carbonate veinlets oblique and parallel to the layering and fine banding (Fig. 32), and in typical streaks of poikiloblastic outgrowths along scapolite-bearing veinlets (Fig. 32) and lithologic banding planes (Fig. 31). In some parquet-structured, sericitized metatuffites scapolite is found as disseminated poikiloblasts enclosing sericite and quartz of the matrix as well as fresh quartz pyroclasts (Figs. 35–37). The smaller of these scapolite poikiloblasts are often round, sometimes with colloform textures (Fig. 33), whereas the larger ones are mostly euhedral (Figs. 35–36). Figures 33–34 show veinlets in the sericitic matrix filled with quartz, feldspar, and chlorite, but the stretches of the veinlets across scapolite poikiloblasts are re-cemented with scapolite. Figures 35–37 show re-cemented fractures in scapolite as seemingly blind scapolite veinlets in scapolite poikiloblasts; a continuation of these scapolite veinlets in the sericitic matrix can sometimes be observed as sericite-overgrown, quartz-feldspar 'ghost' veinlets. The textural observations suggest broadly contemporaneous scapolite blastesis and fracture-filling in soft rocks with well preserved quartz pyroclasts. Rock-fluid equilibrium is suggested by filling of fractures in the matrix with matrix minerals and sealing of fractures in scapolite with scapolite. However, the late formation of chlorite indicates later changes in fluid composition or PT-characteristics.

Paragenetic sequence of structures and textures

Interpretation of textural relations is often ambiguous, e.g., the quartz pyroclasts in Figs. 6–8 resemble quartz pophyroblasts and the albite porphyroblasts in Figs. 25–27 partially resemble recrystallized albite pyroclasts. However, the interpretations gain in strength as they fit into a sequential order corresponding to the crystallization processes envisaged. The structural and textural features of the metatuffites can be interpreted as showing a sequential order involving:

(a) *Relict primary structures of tuffitic sediments.* These include the fine to very fine grain size corresponding to that of volcanic ashes, the fine banding preserving sedimentary structures and pre-diagenetic normal faults and dewatering structures, and the euhedral and angular quartz pyroclasts. These structures are modified or overprinted by later ones.

(b) *Structural features that can be related to prediagenetic alterations.* These include the layer-bound sericitic clay-alterations, micaceous pseudomorphs after clay-altered feldspar pyroclasts, polygonal cracks in quartz pyroclasts, and textures in-

←

Figs. 33–34. Scapolite-bearing sericite-rich metatuffite, slide 106. 33. Small round scapolite poikiloblasts, some with colloform texture (*a*) in parquet-structured sericite; straight veinlet filled with chlorite (black) or quartz-albite (*b*) in stretches across the matrix, and with scapolite (*c*) in stretches across the scapolite poikiloblasts; quartz pyroclast *q* is strained but not fractured. 34. Fracture-filling veinlets with quartz-albite in stretches across the sericite matrix, and scapolite (*c*) in stretches across scapolite poikiloblasts; quartz pyroclast *q* is unaffected by the fracture. All figures with crossed nicols and on same scale.

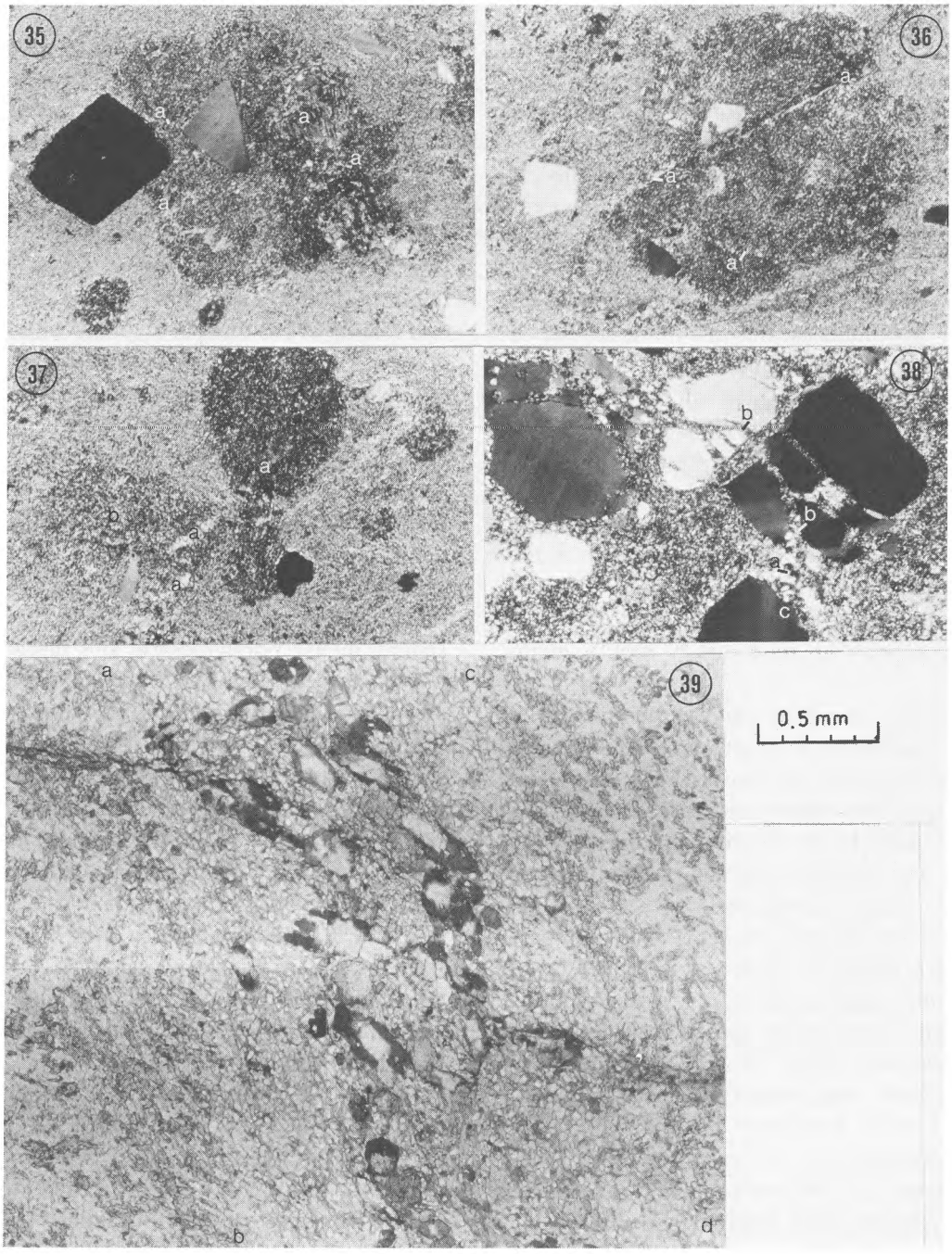

Figs. 35–38. Scapolite-bearing sericite-rich metatuffite, slide 108. 35 and 36. Subhedral, sector-structured scapolite poikiloblasts enclosing fresh quartz pyroclasts; scapolite-recemented fractures appear as seemingly blind veinlets (*a*) across the poikiloblasts, but in fact continue in the matrix as sericite-overgrown quartz-albite 'ghost' veinlets. 37. Scapolite poikiloblasts showing seemingly blind scapolite-recemented veinlets (*a*) along the path of sericite-overgrown 'ghost' veinlets in the matrix; poikiloblast *b* shows inclusions of parquet-structured sericite. 38. Quartz-albite 'ghost' veinlets (*a*) in sericite-quartz-albite matrix traverse fractured quartz pyroclasts as conspicuous quartz-albite veinlets (*b*), but abut against other, unfractured quartz pyroclasts (*c*). All figures with crossed nicols and on same scale.

dicating soft, compressible clay-altered matrix enclosing alteration-resistent, hard quartz pyroclasts.
(c) *Structural features that can be related to syn-diagenetic compaction and recrystallization.* Coeval differential compaction, recrystallization, fracturing and veining is suggested by: parquet, rosette and parallel structures of micas; compaction-related 'ghost' veinlets, blind veinlets, straight and folded cross-veinlets and banding-parallel dilatation veinlets; refracted cross-veinlets; bending of schistosity around blind veinlets and quartz pyroclasts; rotated quartz pyroclasts; compaction-controlled quartz pyroclast fracturing, recrystallization and replacement; and pseudomorphs after quartz pyroclasts.
(d) *Structural features that can be related to late-diagenetic blastesis, recrystallization and metasomatism.* Albite, garnet, scapolite, and other mineral growths sequential to the formation of compaction-related structures are suggested by: poikiloblasts in pseudomorphs after quartz pyroclasts; late mineral growths in and along compaction-related veinlets; disseminated poikiloblasts traversed by compaction-related, often blind veinlets; and coarser grained bands and streaks of late minerals parallel to the differential compaction banding.

A continuous sequential development of minerals and structures should be considered rather than a sharp division in stages. Many recrystallization processes overlap and have occurred throughout two or more stages, e.g. metasomatic alterations are apparent in the late-diagenetic stage, but have also occurred in earlier stages (see below). The syn- and late-diagenetic structures indicate static recrystallization under low lithostatic pressure. With the interpretation of the garnet and scapolite blasts as diagenetic minerals, there is a conspicuous lack of minerals, structures and textures that may be ascribed to later deformation, regional or contact-metamorphism, such as e.g., gneissic structures, shear banding, crenulation and other tectonic microfolds. There is also a lack of reaction textures indicative of typical metamorphic reactions. Instead, a paragenetic sequence of minerals is observed which suggests a control of mineral deposition by hydrothermal fluids evolving through fluid-rock interactions under changing PTX-conditions.

Paragenetic sequence of minerals

The alteration of tuffitic layers involving illitic and other clay mineral precursors of sericite and muscovite is comparable to the potash-bentonitization of felsic volcanic ashes, the clay alterations involving pre-diagenetic metasomatism and K-enrichment. In the diagenetic stage the potash-bentonites recrystallized into sericite-muscovite rocks and the less altered tuffites into quartzo-feldspathic metatuffites. The earlier veinlets in these rocks are 'ghost' veinlets filled with the common rock minerals. 'Ghost' veinlets crossing sericitic, quartzo-feldspathic, and marble bands are often filled with sericite-quartz in the sericitic bands, quartz-albite in the quartzo-feldspathic bands, and carbonate in the marble bands. This banding-related fracture-filling is often very conspicuous and indicates that the composition of the earlier fluids varied with the lithological banding and was controlled by the composition of the rock bands. In other instances, interlayer fluid interactions are suggested by e.g., carbonate-rich veinlets in sericitic and quartzo-feldspathic bands and sericite-quartz-albite-rich veinlets in marbles. The fact that quartz and albite are often fracture-fillings in apparently quartz-albite-depleted sericitic matrix suggest a pressure-solution process of quartz-albite dissolution in the compacting matrix and re-deposition in opening fractures.

Earlier 'ghost' and other veinlets are sometimes overgrown and often intersected by later veinlets of carbonate and/or albite, epidote, amphibole, chlo-

←

Fig. 39. Tremolite-rich metatuffite, slide 513E, A quartzo-feldspathic band (boundaries along *a–b* and *c–d*) is intercalated between tremolite-rich bands; a fracture-filling tremolite-actinolite veinlet crosses the tremolite-rich bands under high angle, but is refracted, kinked and off-set by the apparently stronger compacted quartzo-feldspathic band, which is traversed under lower angle; the veinlet is rather indistinct in the stronger compacted band, the fracture-filling minerals spread out in the latter band and form relatively coarse, zoned tremolite-actinolite crystals, marking the refracted and kinked part of the veinlet; parallel nicols.

rite, and accessory tourmaline, allanite, sphene, and sulfides. Where these veinlets are abundant, quartz pyroclasts are rimmed, veined, and replaced by carbonate and albite. Simultaneously with the subsequent blastesis of albite, garnet, and scapolite in pseudomorphs after quartz pyroclasts, small blasts and spotty or streaky aggregates of albite and/or carbonate, epidote, amphiboles, garnet, and scapolite develop in the matrix of some layers. Some of the blasts and fracture-filling minerals show conspicuous mineral growth zoning (Fig. 39).

Although a pre-diagenetic stage of potash-bentonititzation with formation of clay mineral precursors of sericite-muscovite is assumed, textural evidence suggesting that the late blastic minerals (e.g. garnet, scapolite) may also have formed via a precursor stage, as envisaged by Stanton (1976, 1982), has not been found. The observed textural relations suggest that the late blastic minerals in the tuffite-exhalite sequence were directly precipitated from late evolved metasomatising fluids reacting with rock layers of varied lithological composition. The mineral-depositing fluids evolved from early fluids in equilibrium with the host rocks, to late metasomatising fluids. Changes in PT-conditions may be due to burial and/or volcanic and exhalative activity; changes in fluid composition may result from interlayer fluid-fluid and fluid-rock interactions and mixing with seawater and/or exhaled brine or other hydrothermal waters. The paragenesis of late minerals indicates that the late fluids were enriched in Na (albite, scapolite), Ca (carbonates and calc-silicates), Mg (chlorite), Cl (scapolite), and various minor elements (tourmaline, allanite, sphene, sulfides). The evolved metasomatising fluids reacted with different lithological layers to form minerals characteristic of each different lithology. This is reflected in the metatuffites by the layer-bound distribution of garnet, scapolite, and amphiboles, and to some extent also of epidote, carbonate, and albite. However, lithologically controlled layer-bound metasomatic alterations are especially conspicuous where carbonate, chert, and other exhalite facies intercalations are frequent; these contrasting lithologies often react with the metasomatising fluids to form almost monomineralic rock bands, e.g., albitites, garnetites, tourmalinites, biotite rocks, etc. (see e.g., Plimer, 1986).

Conclusions

The metavolcano-sedimentary rocks in the Bergslagen rift basins locally contain metamorphic minerals like garnet, cordierite and andalusite, which previous authors (e.g., Magnusson, 1925; Lundström, 1985) have always assumed to be products of regional or contact-metamorphism, despite the fact that relations with metamorphic isograds are ambiguous. This widely accepted assumption needs to be re-evaluated in the light of the results of the present paper and new geological models, which ascribe to (sub)seafloor hydrothermal metamorphism an important role in the formation of metaliferous tuffite-exhalite-sediment sequences in riftogenic basins (e.g., Stanton, 1976, 1982, 1987; Hutchinson, 1982, 1983; Plimer, 1986). Variants of the latter models have been proposed for the Bergslagen region by Oen *et al.* (1982), Vivallo & Rickard (1984) and Oen (1987).

The structures and textures of the metatuffites described in the present paper can be interpreted as the result of seafloor, soft rock hydrothermal metamorphism, involving the interaction of different lithologies with hydrothermal fluids of rapidly changing PTX-characteristics; the latter changes may be related to PTX-gradients around exhalative centres and interlayer rock-fluid-seawater-exhalative brine water interactions. The exact PTX-conditions of the syn- to late-diagenetic hydrothermal metamorphism cannot be inferred from the structures and textures, however detailed mineralogical investigations are now in progress. From mineralogical considerations Oen *et al.* (1986) have suggested that peak temperatures of about 400–425° C were locally attained during seafloor hydrothermal metamorphism of stratifrom manganiferous skarns in the Grythyttan basin. In general, however, the rift basin fillings are dominated by low-grade metamorphic rocks with a greenschist facies mineralogy and well preserved sedimentary and volcaniclastic structures. The described tuffite-exhalite sequence of the Vikern-Älvlången area forms part of the homoclinal, steeply SE-dipping, basin-filling succession of the SW Nora half-graben basin (Fig. 40). The Bergslagen graben or rift basins are filled with younger volcano-sedimentary formations (middle

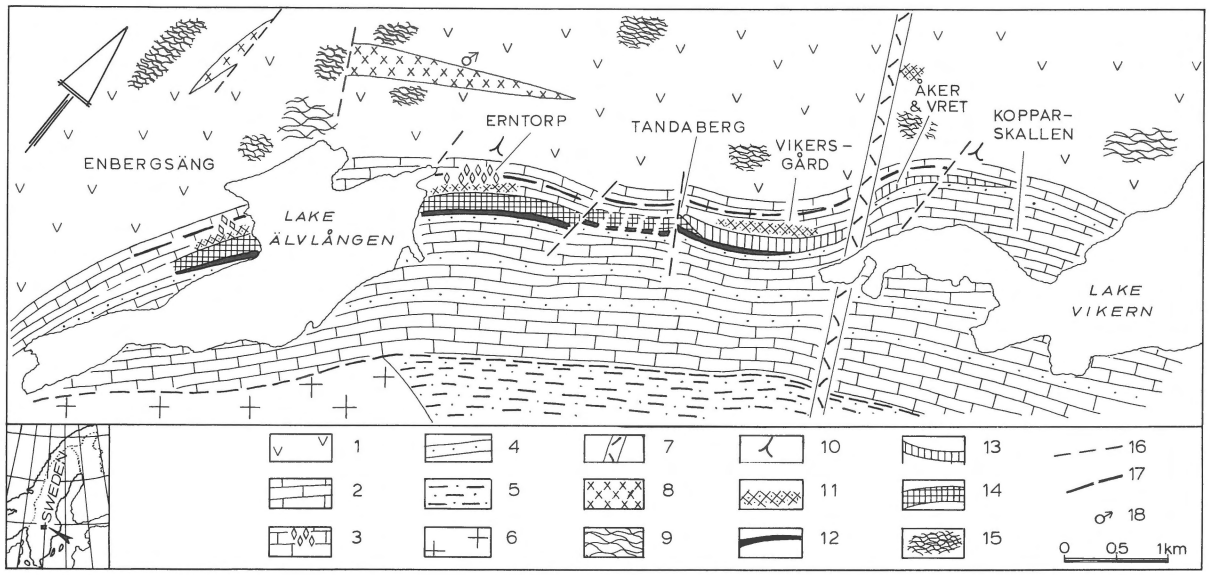

Fig. 40. Geological map of the Vikern-Älvlången area showing the NE-striking, steeply SE-dipping and SE-ward younging homoclinal succession with felsic metavolcanic rocks (1) in the lower, and marbles (2) and metatuffites (5) in the higher part. The felsic metavolcanics (1) show local silicification (9), quartz-tourmaline veins (10), calc-silicate alteration (11), and biotitization (15). The marbles (2) contain intercalations of metatuffites and metacherts (4); near the base of the marbles is a horizon characterized by an alteration of marbles and siliceous, calcareous and pelitic metatuffites, associated with marble breccias (3) and layers of calc-silicate rocks or skarns (11), sphalerite-galena-bearing rocks and ores (12), and garnet-biotite-cummingtonite-(13) and garnet-biotite-rich (14) rocks. Samples described in this paper are from metatuffites in the latter horizon. Other rock units shown are a Filipstad-type granite (6), a dolerite dyke (7), and metabasites (8); also shown are minor (16) and major (17) faults and an occurrence of banded iron formation (18).

leptite and upper leptite and slate groups) of the Bergslagen supracrustal sequence (Oen, 1987). A model for the evolution of the Bergslagen rift basins depicting simultaneous graben or half-grabem formation, sedimentation, and passive rotation into steep homoclinal to vertical position of the basin-filling sequences, due to the foundering and rotation of the basin floor, has been proposed by Kuipers (1987). The metavolcano-sedimentary rocks of the rift basins have not been subjected to post-basinal folding, penetrative deformation or regional metamorphism, and they show essentially the imprints of syn-diagenetic seafloor hydrothermal metamorphic processes. Although in the SW Nora basin cordierite and andalusite have not been found, the peculiar stratabound occurrence of these minerals in the youngest seafloor hydrothermal metamorphosed formations of other Bergslagen rift basins, such as the Saxån (Magnusson, 1925) and Ställdalen (Lundström, 1985) basins, suggests that interesting new conclusions may be expected from a re-investigation and critical re-evaluation of the metamorphic-petrologic aspects of especially these cordierite and andalusite occurrences in a rift basin setting.

The older rocks (lower and middle leptite groups) of the basin floors may have been subjected to similar syn-diagenetic alterations as those of the younger rocks, but here the early alterations are overprinted by post-diagenetic deeper burial metamorphism and later subseafloor hydrothermal alteration. These rocks often show the typical 'leptite structure' of granoblastic metavolcanites with often well preserved primary volcanic rock structures such as pyroclasts, shards, phenocrysts, and flow banding. The latter structures are often internally recrystallized in granular aggregates with preservation of the external structural forms, e.g., recrystallized quartz pyroclasts resembling the ones described in this paper are common in some

leptites. The so-called leptites show a typical kind of annealing texture, which may be characteristic of the deeper burial and subseafloor metamorphism in specific geological settings of the Bergslagen region. Since the conditions of the latter metamorphism may approach those of low-pressure, medium-grade regional metamorphism, structures (e.g., gneissose structures, crenulation folds), textures (e.g., porphyroblasts), and minerals (local cordierite, andalusite, garnet, amphibole) resembling those found in regional metamorphic rocks are locally also common in the leptites.

Acknowledgements

The authors are indebted to R. Lilljequist, SGAB project-manager, for an instructive field excursion and fruitful discussion; to R.H. Verschure of the ZWO-Laboratorium voor Isotope- Geologie, Amsterdam, for X-ray determination of scapolite; and to W.J. Lustenhouwer of the ZWO-WACOM working group for analytical geochemistry, for microprobe analyses of garnet and scapolite.

References

Davison, I. 1987 Normal fault geometry related to sediment compaction and burial – J. Struct. Geol. 9: 393–401.

Hellingwerf, R.H., Lilljequist, R. & Ljung, S. 1988 Stratiform Zn-Pb-Fe-Mn mineralization in the Alvlången-Vikern area, Bergslagen, Sweden. In: Baker, J.H. & R.H. Hellingwerf (eds): The Bergslagen Province, Central Sweden – Stratigraphy and ore-forming processes. I.G.C.P. project 247 – Geol. Mijnbouw 67: 313–332 (this issue).

Hutchinson, R.W. 1982 Syn-depositional hydrothermal processes and Precambrian sulphide deposits – In: Hutchinson, R.W., Spence, C.D. & Franklin, J.M. (eds): Precambrian sulphide deposits – Geol. Assoc. Can. Spec. Pap. 25: 761–791.

Hutchinson, R.W. 1983 Hydrothermal concepts: the old and the new – Econ. Geol. 78: 1734–1741.

Kuipers, G. 1987 Volcaniclastic facies associations in the Mid-Proterozoic Grythyttan rift-basin and their lithostratigraphic relationship, West Bergslagen, central Sweden – Ph.D. Thesis Univ. of Amsterdam, GUA Papers of Geology I–28: 162 pp.

Lundström, I. 1985 Beskrivning till Berggrundskartan Lindesberg NV – Sver. Geol. Unders. Ser. Af 140: 131 pp.

Magnusson, N.H. 1925 Persberg malmtrakt – Beskr. Mineralfyndigheter 2, Kungl. Kommerskoll. Stockholm: 231 pp.

Miyano, T. 1982 Stilpnomelane, iron-rich mica, K-feldspar and hornblende in banded iron-formation assemblages of the Dales Gorge Member, Hamersley Group, Western Australia – Can. Miner. 20: 189–202.

Oen, I.S. 1987 Rift-related igneous activity and metallogenesis in SW Bergslagen, Sweden – Precambr. Res. 35: 367–382.

Oen, I.S., Helmers, H., Verschure, R.H. & Wiklander, U. 1982 Ore deposition in a Proterozoic incipient rift zone environment: a tentative model for the Filipstad-Grythyttan-Hjulsjö region, Bergslagen, Sweden – Geol. Rundsch. 71: 182–194.

Oen, I.S., De Maesschalck, A.A. & Lustenhouwer, W.J. 1986. Mid-Proterozoic exhalative-sedimentary Mn-skarns containing possible microbial fossils, Grythyttan, Bergslagen, Sweden – Econ. Geol. 81: 1533–1543

Plimer, I.R. 1986 Sediment-hosted exhalative Pb–Zn deposits, products of contrasting ensialic rifting – Trans. Geol. Soc. S. Africa 89: 57–73.

Stanton, R.L. 1976 Petrochemical studies of ore environment, Broken Hill, New South Wales, Australia: 1 – Constitution of 'banded iron formation'; 2 – Regional metamorphism of banded iron formations and their immediate associates; 3 – Banded iron formations and sulphide ore bodies: constitutional and genetic ties; 4 – Environmental synthesis – Trans. Inst. Min. Metall. Sect B Appl. Earth Sci. 85: 33–46, 118–131, 132–141, 221–233.

Stanton, R.L. 1982 Metamorphism of a stratiform sulphide ore-body at Mount Misery, Einasleigh, Queensland, Australia: 1 Observations, 2 Implications – Trans. Inst. Min. Metall. Sect. B Appl. Earth Sci. 91: 47–80.

Stanton, R.L. 1987 Constitutional features, and some exploration implications, of three zinc-bearing stratiform skarns of eastern Australia – Trans. Inst. Min. Metall. Sect. B Appl. Earth Sci. 96: 37–57.

Van Loon, A.J. & Brodzikowski, K. 1987 Problems and progress in the research on soft-sediment deformation – Sediment. Geol. 50: 167–193.

Vivallo, W. & Rickard, D. 1984. Early Proterozoic ensialic spreading-subsidence: evidence from the Garpenberg enclave, central Sweden – Precambr. Res. 26: 203–221.